



HAL
open science

Confined directional drying of a colloidal dispersion: kinetic modeling

Hrishikesh Pingulkar, Jean-Baptiste Salmon

► **To cite this version:**

Hrishikesh Pingulkar, Jean-Baptiste Salmon. Confined directional drying of a colloidal dispersion: kinetic modeling. *Soft Matter*, 2023, 19 (12), pp.2176-2185. 10.1039/d3sm00058c . hal-04247245

HAL Id: hal-04247245

<https://hal.science/hal-04247245v1>

Submitted on 18 Oct 2023

HAL is a multi-disciplinary open access archive for the deposit and dissemination of scientific research documents, whether they are published or not. The documents may come from teaching and research institutions in France or abroad, or from public or private research centers.

L'archive ouverte pluridisciplinaire **HAL**, est destinée au dépôt et à la diffusion de documents scientifiques de niveau recherche, publiés ou non, émanant des établissements d'enseignement et de recherche français ou étrangers, des laboratoires publics ou privés.

Cite this: DOI: 00.0000/xxxxxxxxxx

Confined directional drying of a colloidal dispersion: kinetic modeling[†]

Hrishikesh Pingulkar^a and Jean-Baptiste Salmon^a

Received Date

Accepted Date

DOI: 00.0000/xxxxxxxxxx

We derive a model to describe the dynamics of confined directional drying of a colloidal dispersion. In such experiments, a dispersion of rigid colloids is confined in a capillary tube or a Hele-shaw cell. Solvent evaporation from the open end accumulates the particles at the tip up to the formation of a porous packing that invades the cell at a rate $\frac{dl}{dt}$. Our model based on a classical description of fluid mechanics and capillary phenomena, predicts different regimes for the growth of the consolidated packing, l versus t . At early times, the evaporation rate is constant and the growth is linear, $l \propto t$. At longer times, the evaporation rate decreases and the consolidated packing grows as $l \propto \sqrt{t}$. This slowdown is either related to the recession of the drying interface within the packing thus adding a resistance to evaporation (*capillary-limited regime*), or to the Kelvin effect which decreases the partial pressure of water at the drying interface (*flow-limited regime*). We illustrate these results with numerical relations describing hard spheres, showing that these regimes are a priori experimentally observable. Beyond this description of the confined directional drying of colloidal dispersions, our results also highlight the importance of relative humidity control in such experiments.

1 Introduction

The drying of colloidal dispersions, allowing by simple evaporation of a solvent to form a dense and consolidated material from colloids dispersed in a liquid, is a key step of many industrial processes, from coatings to electrode manufacturing.^{1,2} The detailed understanding of the mechanisms at play remains a scientific challenge and involves multiple aspects: transport phenomena, physical chemistry of colloids, mechanical instabilities, etc.^{3–6}

In this context, different studies have used a simplified geometrical configuration known as *confined directional drying* to provide a better understanding. Figure 1 shows these experiments schematically: a horizontal capillary tube or a Hele-Shaw cell, with a cross-sectional dimension h typically less than 100 μm , is filled by an aqueous colloidal dispersion and open on one side to the ambient atmosphere with relative humidity RH. As long as capillary forces pin the air-water interface at the open end of the cell, evaporation causes a flow at a volumetric rate J (m^3/s):

$$J = \frac{1}{A\rho_w} \frac{dM}{dt}, \quad (1)$$

to replenish the lost water mass $\frac{dM}{dt}$ (kg/s), A (m^2) being the cross-sectional area of the cell and ρ_w (kg/m^3) the mass density of liquid water. This flow continuously accumulates the colloids

at the tip until the formation of a consolidated close-packed network. For rigid colloids, the porosity of this layer does not prevent evaporation, and thus its growth at a rate $\frac{dl}{dt}$, see Fig. 1. This configuration shares various similarities with the more general *directional drying* often observed for liquid films deposited on a substrate,^{7,8} but with the notable difference that evaporation occurs here only through the end of the tube, and thus only through the colloidal packing. In this sense, confined directional drying is fundamentally closer to configurations such as drying of quiescent films,^{9,10} i.e., without lateral flows induced by edge effects, or drying of 2D and 3D drops, for which evaporation also occurs only through the consolidated colloids.^{11–14} The same remark also applies to the classical case of sessile drops, for which several ingredients presented in Fig. 1 also apply, but with the difference of the finite volume of dispersion and the complexity associated with the possible deformation of the evaporation surface during drying.¹⁵

Confined directional drying has been widely used to study the fracture patterns induced by drying,^{16–21} the phenomenon of delamination,^{22,23} or the appearance of shear bands.^{24,25} Beyond these issues concerning mechanical instabilities, this technique has also been used to study mass transport in colloid dispersions,^{26–29} the formation of an amorphous solid prior to consolidation,³⁰ or the mechanisms of colloidal ordering.^{31,32}

In spite of all these works, one fundamental question remains unanswered: that of the growth kinetics of the colloidal packing, l as a function of t . Experiments have shown that the growth

^a CNRS, Solvay, LOF, UMR 5258, Univ. Bordeaux, F-33600 Pessac, France

is linear, $l \propto t$, for colloids with large radii ($a > 100 \text{ nm}$ ³³), as expected from mass conservation^{34,35} for a constant evaporation rate J . For smaller colloids, typically $a < 20 \text{ nm}$, a transition towards a square root growth, $l \propto \sqrt{t}$, has often been reported at longer times, suggesting a slowdown of the evaporation rate.^{17,18,20,22} Dufresne et al. were the first to propose a law able to fit all the $l(t)$ observations, and explained the transition from $l \propto t$ to $l \propto \sqrt{t}$, by invoking a transition from an *evaporation-limited* to a *flow-limited* regime.¹⁷ Their model also showed that the crossover between these two regimes occurred for a critical length l_c scaling linearly with the colloid size $l_c \sim a$, in conflict with the experimental data.¹⁷ Furthermore, the derivation of this law was empirical, and the same authors later proposed¹⁸ that the square root slowdown was actually probably due to the recession of the air–water interface within the porous colloidal packing over a small length ξ , as shown in Fig. 1(b). Wallenstein and Russel then suggested theoretically that Knudsen diffusion of water vapor through the dry porous layer results in a very strong resistance to mass transfer, leading to a slowing of the evaporation rate J and a square root growth of the front, $l \propto \sqrt{t}$, but with a tiny recession, $\xi \ll l$.³⁶

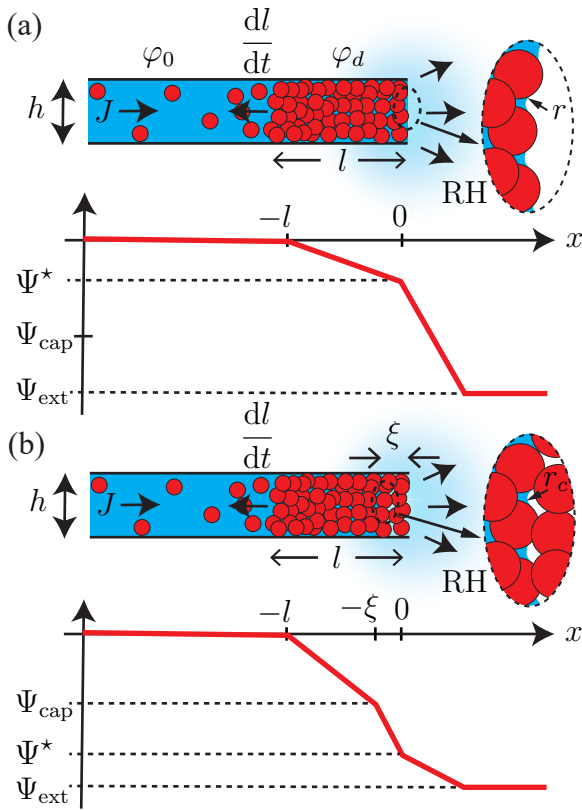


Fig. 1 Confined directional drying of a colloidal dispersion. (a) Capillary forces hold the air-water menisci (radius of curvature r) at the outlet of the cell. (b) Recession of the evaporation interface within the colloidal packing, leading to a dry layer of thickness ξ (radius of curvature r_c). The water potential profiles are shown below for both scenarios.

Later, Lidon et al. showed that the Kelvin effect, i.e., the decrease in the partial pressure of water due to highly curved menisci at the drying interface, see Fig. 1, should probably also

be taken into account, especially for colloids with small radii a .³⁷ Their model, including also the possible recession of the drying interface, now predicted that the crossover length scales as $l_c \sim a^2$, possibly explaining the discrepancies between experiments and models pointed out by Dufresne et al.¹⁷ Importantly, their model incorrectly assumed that the ambient relative humidity RH was strictly zero. As shown below, this model cannot describe with this assumption the existence of the *flow-limited* regime suggested in Ref.¹⁷ This error was recently revealed by Tatsumi et al. who developed a model to describe the drying of quiescent colloidal films.³⁸ This model, of which some relations are resumed below, does not take into account the possible recession of the interface in the packing, and therefore cannot describe part of the regimes detailed in the present work.

The primary motivation of our work is to clarify the description of the kinetics, l versus t , using a simple model of confined directional drying of a colloidal dispersion. Our model takes into account both the Kelvin effect and the possible recession of the evaporation interface, and applies continuously to colloids with radii ranging from a few nanometers to a few hundreds of nanometers. As shown below, this model highlights the importance of RH on the growth kinetics of the dense packing, and reveals the existence of two distinct regimes to explain the square root growth $l \propto \sqrt{t}$. Beyond the very specific geometry of confined directional drying described in Fig. 1, the ingredients of our model also apply a priori to any drying configuration of colloidal dispersions (including also those of finite volume such as the drying of sessile droplets and films), when the Kelvin effect, but also capillary effects come into play by modifying the evaporation conditions. To our knowledge, these ingredients are rarely taken into account, and the evaporation rate is often described as not depending on the presence of closely-packed colloids.

The present paper is organized as follows. In Sec. 2, we first present the main assumptions of our model and the equations governing the growth rate $\frac{dl}{dt}$. In Sec. 3, we then present the main results of this model including the different growth regimes, and discuss the role played by relative humidity. Finally, we illustrate the model on a relevant experimental case using standard relations valid for monodisperse hard-spheres. In Sec. 4, we conclude our work by suggesting possible experiments and research directions to improve the model.

2 Model

2.1 Geometry, assumptions, and water potential

We consider the configuration shown in Fig. 1(a). The cell is initially filled by a dispersion of colloids with radii $a \ll h$, at a volume fraction φ_0 . We consider that colloids cannot adhere to the cell walls in the dispersed state. We also assume that colloids are rigid and cannot deform upon accumulation. The volume fraction φ_d of the dense packing is thus considered uniform and constant. To model the growth rate of the packing, we consider for simplicity a one-dimensional description and isothermal conditions. We also assume the local thermodynamic equilibrium and quasi-static conditions for writing the different fluxes driven by evaporation.

In the following, we use the water potential Ψ (Pa) because

it allows a convenient description of water independently of its thermodynamic state: liquid in the dispersion and in the pores of the colloidal packing, to vapor in the ambient air. The latter is defined by:

$$\Psi = \frac{\mu - \mu_0(T)}{V_m}, \quad (2)$$

where $\mu = \mu(P, T)$ is the water chemical potential expressed in units of J/mol at pressure P (Pa) and absolute temperature T (K), $\mu_0(T)$ is its standard value at atmospheric pressure P_0 and sea level, and $V_m(P, T)$ is the liquid water molar volume ($V_m \simeq 1.805 \times 10^{-5} \text{ m}^3/\text{mol}$ at P_0 and room temperature, $T = 22^\circ\text{C}$).

In ambient air, far from the outlet, the water potential is given by:

$$\Psi_{\text{ext}} = \frac{RT}{V_m} \log(\text{RH}), \quad (3)$$

R being the universal gas constant. Because colloidal interactions in the dilute dispersion lead to a negligible water potential compared to the other potentials considered later,³⁹ one has $\Psi \simeq 0$ upstream $x = -l$. Water evaporation results from the drop of the water potential from $\Psi \simeq 0$ to Ψ_{ext} , see Fig. 1.

Importantly, we will assume below a classical description of fluid mechanics and capillary phenomena down to nanometer-sized colloids. This assumption is based on the results of Vincent et al. on evaporation-induced flows through nano-porous media,⁴⁰ who showed that a classical description remains valid even with pore radii $r_p \simeq 1.7 \text{ nm}$. Furthermore, the problem studied by Vincent et al. shares many similarities with the case shown in Fig. 1, but in a static configuration (the size of the porous medium being fixed), and several equations described below have already been discussed in Ref.⁴⁰

2.2 Evaporation rate

Two configurations emerge depending on the strength of the capillary forces: fully wetted colloidal packing, Fig. 1(a), or recession of the air-water interface, Fig. 1(b).

2.2.1 No recession

In Fig. 1(a), capillary forces are strong enough to avoid the recession of the air-water menisci in the porous network. In this regime, the global mass balance imposes a flow in the cell and through the whole porous packing. This flow depends on two resistances in series for the drop in water potential: vapor removal in ambient air and liquid water flow through the porous layer. Evaporation rate in ambient air is described assuming quasi-steady conditions by:⁴¹

$$J = \frac{kc_{\text{sat}}}{\rho_w} (\text{RH}^* - \text{RH}), \quad (4)$$

where RH^* is the relative humidity at the evaporation interface ($x = 0$) and c_{sat} (kg/m³) the water concentration at saturation in air. k (m/s) is a mass transfer coefficient that accounts for the transport of the vapor by diffusion and convection in air.

The evaporation-induced flow leads to a drop of water potential

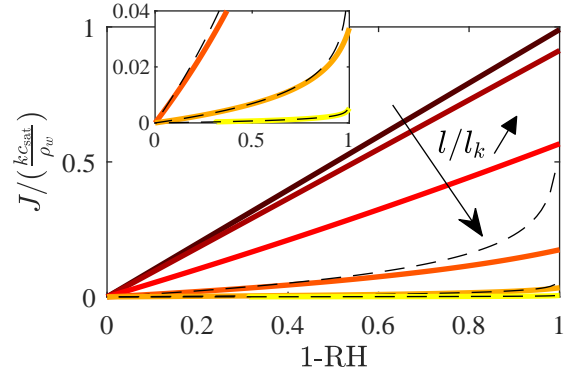


Fig. 2 Evaporation rate given by Eqs. (4) and (8) versus $1 - \text{RH}$, for $l/l_k = 10^{-2}, 10^{-1}, 1, 10, 10^2,$ and 10^3 . Inset: zoom for the high values of l/l_k . The dotted lines are the approximations Eq. (11) for $l \gg l_k$.

due to the viscous friction given by the Darcy's law:

$$\Psi^* = -\frac{\eta_w l}{\kappa} J, \quad (5)$$

where η_w (Pa s) is the water viscosity and κ (m²) the permeability of the colloidal packing. We neglect in this description the drop in water potential due to the hydraulic resistance of the cell itself, an assumption fully justified since $a \ll h$.

Kelvin's relation, i.e., the continuity of the water potential at the air-water interface, relates RH^* to Ψ^* :

$$\text{RH}^* = \exp\left(\frac{V_m \Psi^*}{RT}\right), \quad (6)$$

and the radius of curvature $r > 0$ of the menisci, see Fig. 1(a), is given by the Kelvin-Laplace equation:

$$\Psi^* = -\frac{2\gamma}{r}, \quad (7)$$

where γ (N/m) is the air-water surface tension. Equations (6) and (7) show that RH^* deviates from $\text{RH}^* = 1$ only for water potential drops $-\Psi^*$ that are not negligible compared to RT/V_m ($\simeq 136 \text{ MPa}$ at $T = 22^\circ\text{C}$), and thus radii of curvature typically less than $r \leq 10 \text{ nm}$ considering $\gamma \simeq 70 \text{ mN/m}$.

Using Eqs. (4), (5), and (6), one can show that:

$$\text{RH}^* = \frac{l_k}{l} W \left[\frac{l}{l_k} \exp\left(\text{RH} \frac{l}{l_k}\right) \right], \quad (8)$$

with the length scale l_k defined by :

$$l_k = \left(\frac{\kappa(RT/V_m)}{\eta_w} \right) / \left(\frac{kc_{\text{sat}}}{\rho_w} \right), \quad (9)$$

and W the Lambert W -function,⁴² the inverse function of $f(w) = w \exp(w)$, i.e., $z = w \exp(w) \Leftrightarrow w = W(z)$.

Figure 2 shows the evaporation rate given by Eq. (4) with RH^* calculated using Eq. (8) versus $(1 - \text{RH})$ and for various values of l/l_k . For $l \ll l_k$, the Taylor series⁴² of W in Eq. (8) leads to $\text{RH}^* \simeq 1$, so that evaporation is limited by the rate of vapor removal in

the ambient air and thus:

$$J \simeq \frac{kc_{\text{sat}}}{\rho_w} (1 - \text{RH}). \quad (10)$$

For $l \gg l_k$, the asymptotic expansion⁴² of W in Eq. (8) shows that $\text{RH}^* \simeq \text{RH}$, and Eq. (5) leads to:

$$J \simeq -\frac{\kappa}{\eta_w l} \Psi_{\text{ext}} = -\frac{kc_{\text{sat}} l_k}{\rho_w l} \log(\text{RH}). \quad (11)$$

In this case, evaporation is limited by the flow through the porous layer and does not depend anymore on the mass transfer coefficient k in ambient air.⁴⁰

2.2.2 Meniscus recession

When capillary forces are no longer able to maintain the pinning of the menisci at $x = 0$, the air-water interface recedes in the porous packing, see Fig. 1(b). This recession occurs when the radii of curvature reach a critical value r_c , or equivalently when the drop in water potential Ψ^* reaches the maximal capillary pressure $\Psi_{\text{cap}} = -2\gamma/r_c$.

In this regime, there is an additional resistance to evaporation due to the transport of the water vapor in the dry porous layer of thickness ξ . To model this case, we first assume that the rate of recession is small compared to the rate of water mass loss $\frac{dM}{dt}$. Equation (1) thus remains valid for estimating the evaporation-induced flow J , and we will discuss later this assumption in more detail.

We also assume homogeneous recession over the cross-section of the porous layer. This corresponds to neglecting the pore size distribution (equivalently, the critical radii r_c) of the colloidal packing which would lead to the existence of a partially saturated layer, due to the preferential emptying of the largest pores.⁴³ For simplicity, we do not consider this possibility often observed for the drying of porous media,^{44,45} and our model actually applies only to cases where the partially saturated layer has negligible width.

In the ambient air, Eq. (4) still relates the vapor removal rate to the evaporation-induced flow J . The transport of the water vapor through the dry porous layer is limited by diffusion, and the global mass balance imposes:

$$J = \frac{D_w^p c_{\text{sat}}}{\rho_w \xi} (\text{RH}_{\text{cap}} - \text{RH}^*), \quad (12)$$

where D_w^p is the effective diffusion coefficient of the water vapor in the porous medium, RH^* the relative humidity at $x = 0$, and RH_{cap} the relative humidity at $x = -\xi$ linked to Ψ_{cap} by the Kelvin relation. Finally, the flow J leads to a drop in water potential across the porous layer given by:

$$J = -\frac{\kappa \Psi_{\text{cap}}}{\eta_w (l - \xi)}. \quad (13)$$

Equations (4), (12), and (13) can be used to show that:

$$\frac{\xi}{l} = \frac{\text{RH}_{\text{cap}} - \text{RH} - (D_w^p \Gamma)/(kl)}{\text{RH}_{\text{cap}} - \text{RH} + \Gamma}, \quad (14)$$

with the dimensionless parameter:

$$\Gamma = -\left(\frac{\kappa \Psi_{\text{cap}}}{\eta_w}\right) / \left(\frac{D_w^p c_{\text{sat}}}{\rho_w}\right). \quad (15)$$

Γ compares the flux of liquid water driven by the capillary pressure Ψ_{cap} across a given thickness L of the porous layer [$\kappa \Psi_{\text{cap}}/(\eta_w L)$] to the flux of liquid water driven by the diffusion of water vapor over the same thickness [$D_w^p c_{\text{sat}}/(\rho_w L)$]. As shown in Sec. 3.3.2 with numerical applications, $\Gamma \gg 1$ regardless of the colloid size a . Because the numerator in Eq. (14) is smaller than $\text{RH}_{\text{cap}} - \text{RH} \leq 1$, $\Gamma \gg 1$ implies $\xi \ll l$, and Eq. (13) shows that the evaporation rate can be approximated by:

$$J \simeq -\frac{\kappa}{\eta_w l} \Psi_{\text{cap}}. \quad (16)$$

2.3 Growth of the porous layer

The flow J driven by evaporation continuously accumulates colloids to the porous packing, which consequently invades the cell at a given rate. The growth dynamics, l versus t , depends on multiple phenomena such as the transport of the colloids by advection up to the packing, diffusion which opposes the formation of concentration gradients upstream $x = -l$, but also on the consolidation dynamics of colloids in the packing.

Despite this complexity, the growth rate is often described in the literature,^{17,20,36–38} by the simplified colloid mass balance:

$$(\varphi_d - \varphi_0) \frac{dl}{dt} \simeq \varphi_0 J. \quad (17)$$

This relation neglects, however, any temporal evolution of the colloid concentration profile in the dispersion upstream $x = -l$. In Sec. 3.3.1, we show using a simple transport model for the colloidal dispersion, that these variations are small, and that Eq. (17) correctly describes the growth rate of the dense packing. Moreover, Eq. (17) combined with the weak recession of the air-water menisci, $\xi \ll l$ (coming from the assumption $\Gamma \gg 1$), leads to $\frac{d\xi}{dt} \ll J$. This confirms that the rate of menisci recession makes a negligible contribution to the mass loss $\frac{dM}{dt}$, and that the evaporation-induced flow J remains correctly given by Eq. (1) in this regime.

2.4 Dimensionless model

For clarity, we define the dimensionless quantities:

$$\tilde{l} = \frac{l}{l_k}, \quad \tilde{t} = \frac{t}{t_k}, \quad \text{and} \quad j = \frac{J}{J_0}, \quad (18)$$

with:

$$J_0 = \frac{kc_{\text{sat}}}{\rho_w}, \quad t_k = \frac{l_k}{J_0} \frac{\varphi_d - \varphi_0}{\varphi_0}, \quad (19)$$

and l_k defined in Eq. (9). With these dimensionless variables, our model for the growth dynamics is simply written:

$$\frac{d\tilde{l}}{d\tilde{t}} = j. \quad (20)$$

In the regime of no recession, i.e., when $\Psi^* > \Psi_{\text{cap}}$, Eqs. (4)

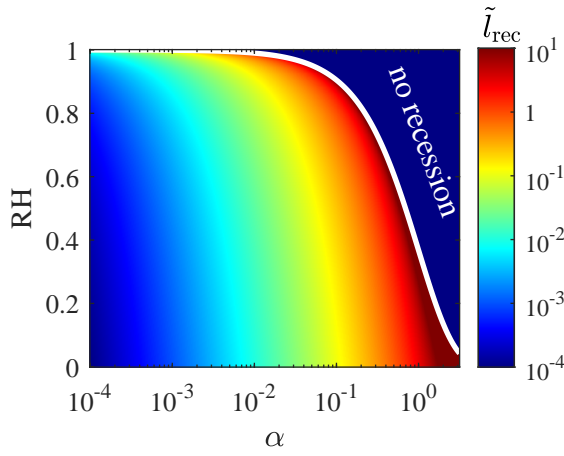


Fig. 3 Critical length \tilde{l}_{rec} (in log scale) given by Eq. (25) in the plane α -RH. The white line given by $\alpha = -\log(\text{RH})$ delimits the zone of menisci recession, see Eq. (24).

and (8) lead to the normalized evaporation rate:

$$j = \frac{1}{\tilde{l}} W [\tilde{l} \exp(\text{RH} \tilde{l})] - \text{RH}. \quad (21)$$

When $\Psi^* < \Psi_{\text{cap}}$, the air/water interface recedes, and j given by Eq. (16) is now simply written:

$$j = \frac{\alpha}{\tilde{l}}, \quad (22)$$

with

$$\alpha = -\frac{\Psi_{\text{cap}}}{RT/V_m}, \quad (23)$$

a dimensionless parameter comparing the capillary pressure Ψ_{cap} to RT/V_m , the characteristic pressure scale of the Kelvin effect.

3 Results and Discussion

3.1 Condition for recession of the interface

In the kinetic model described in the previous section, the recession of the menisci never occurs when the critical capillary pressure is smaller than the water potential in the ambient air, i.e., when $\Psi_{\text{cap}} < \Psi_{\text{ext}}$, see Fig. 1. With the notation of Eq. (23), this condition reads:

$$\alpha > -\log(\text{RH}). \quad (24)$$

When Eq. (24) is not fulfilled, the menisci recede within the porous layer when Ψ^* reaches Ψ_{cap} . Equations (5) and (21) then show that it occurs for the critical length:

$$\tilde{l}_{\text{rec}} = \frac{\alpha}{\exp(-\alpha) - \text{RH}}. \quad (25)$$

Figure 3 shows \tilde{l}_{rec} in the plane α -RH. The regime for which the menisci never recede is expected only at high relative humidity and for large α values. For standard conditions, this regime corresponds to high values of the capillary pressure Ψ_{cap} , since $RT/V_m \simeq 136$ MPa at $T = 22^\circ\text{C}$. According to the Kelvin-Laplace

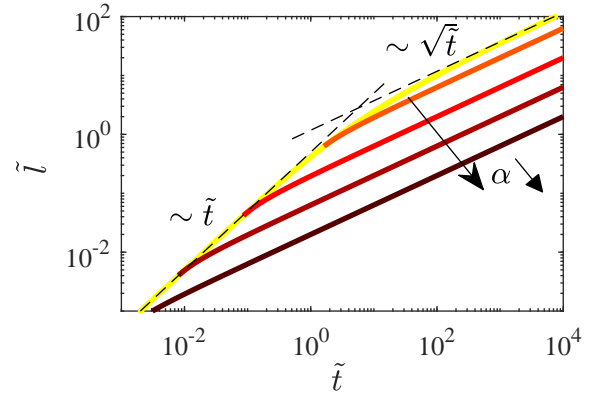


Fig. 4 Yellow: numerical solution of Eq. (20) for $\text{RH} = 0.5$. The dashed lines show the approximation Eq. (27) at low \tilde{t} , and the flow-limited regime Eq. (28) at larger \tilde{t} . The other curves are given by Eq. (30) for $\alpha = 2 \times 10^{-1}, 2 \times 10^{-2}, 2 \times 10^{-3},$ and 2×10^{-4} (from orange to brown).

equation Eq. (7), this corresponds to very small critical radii, typically $r_c \simeq 1.5$ nm for $\text{RH} = 0.5$ assuming the surface tension is $\gamma \simeq 70$ mN/m. Such cases are therefore only expected for colloids with radii $a \leq 10$ –20 nm, as in some experimental studies cited above.^{17,18,37} As mentioned previously, Vincent et al. studied the drying-induced flows through a porous silicon layer with pore radius $r_p \simeq 1.7$ nm.⁴⁰ These experiments share various similarities with the problem studied here, but in a static configuration. The experiments of Vincent et al., corresponding to $\alpha \simeq 0.6$ with our notations, clearly revealed drying-induced flows given by Eq. (11) for high RH, and recession of the menisci at lower RH, leading to capillarity-limited flows, Eq. (16).

In the case of larger colloids, typically $a \gg 20$ nm, one has $\alpha \ll 1$, and Eq. (25) turns into real units in:

$$l_{\text{rec}} \simeq -\frac{\kappa}{\eta_w} \frac{\Psi_{\text{cap}}}{J_0(1 - \text{RH})}. \quad (26)$$

As expected, this relation does not involve anymore the characteristic pressure scale RT/V_m , and could have been derived without invoking the Kelvin effect.

3.2 Growth dynamics

Figure 4 shows the numerical solutions of the ordinary differential equation Eq. (20) for $\text{RH} = 0.5$ and different α values, with the initial condition $\tilde{l} = 0$ at $\tilde{t} = 0$. When the condition Eq. (24) is fulfilled, j is given by Eq. (21), while for the other cases, Eq. (20) is solved with j given by Eq. (21) for $\tilde{l} \leq \tilde{l}_{\text{rec}}$, and with j given by Eq. (22) for $\tilde{l} > \tilde{l}_{\text{rec}}$.

We first focus on the regime of no recession (yellow curve in Fig. 4). For $\tilde{l} \ll 1$, the evaporation rate is constant and well-approximated by Eq. (10) ($j \simeq 1 - \text{RH}$ with the dimensionless variables), so that the length of the porous layer grows linearly following:

$$\tilde{l} \simeq (1 - \text{RH}) \tilde{t}. \quad (27)$$

At longer times scales, the evaporation rate decays due to the decrease in water potential at the evaporation interface. For $\tilde{l} \gg 1$,

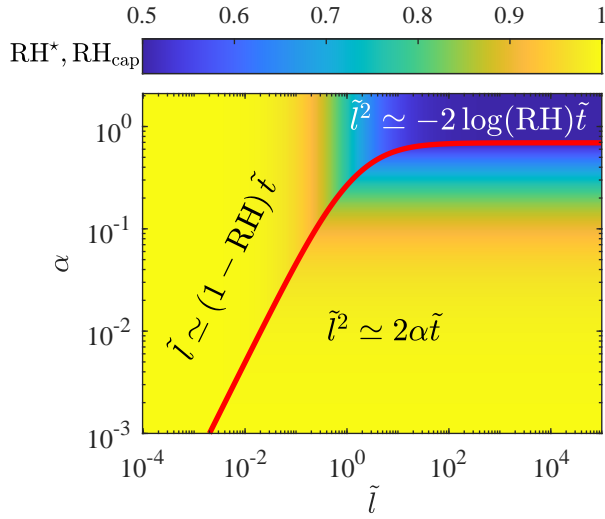


Fig. 5 Case $RH = 0.5$. Colors code for the relative humidity at the evaporation interface (RH^* when no recession, RH_{cap} in the other case). The red line is Eq. (25) and delimits the regime of menisci recession from that of no recession.

Eq. (11) shows that the evaporation rate follows approximately $j \simeq -(1/\tilde{l})\log(RH)$, leading to the square root growth:

$$\tilde{l}^2 \simeq -2\log(RH)\tilde{t}. \quad (28)$$

The transition from the *evaporation-limited* regime given by Eq. (27) to the *flow-limited* regime given by (28) occurs at the length:

$$\tilde{l}_{\text{kel}} \simeq \frac{-2\log(RH)}{1 - RH}, \quad (29)$$

with the subscript *kel* to emphasize that the origin of the square root growth at long times is due to the Kelvin effect.

When the condition Eq. (24) is not fulfilled, the growth first follows the same \tilde{l} versus \tilde{t} curve up to $\tilde{l} = \tilde{l}_{\text{rec}}$ given by Eq. (25). At later times, the length of the porous layer grows as:

$$\tilde{l}^2 = \tilde{l}_{\text{rec}}^2 + 2\alpha(\tilde{t} - \tilde{t}_{\text{rec}}), \quad (30)$$

and thus:

$$\tilde{l}^2 \simeq 2\alpha\tilde{t}, \quad (31)$$

for $\tilde{l} \gg \tilde{l}_{\text{rec}}$. Equation (30) has already been derived by Wallenstein and Russel,³⁶ but without taking into account the Kelvin effect, and thus the possible decrease of the evaporation-driving force for small curvature radii. Later, Lidon et al. found again Eq. (30) now taking into account the Kelvin effect,³⁷ but assuming $RH = 0$ and thus missing the description of the flow-limited regime described above, as revealed recently by Tatsumi et al.³⁸

Figure 5 summarizes on a single diagram in the plane \tilde{l} - α , the different asymptotic regimes of growth of the packing for a fixed RH , as well as the values of the relative humidity at the air-water interface. This diagram helps to reveal that the model always predicts a linear growth $\tilde{l} \propto \tilde{t}$ at early times followed by a square root slowing down $\tilde{l}^2 \propto \tilde{t}$ but with two different origins.

For $\alpha < -\log(RH)$, the slowing down occurs due to the minute recession of the interface that adds a resistance to evaporation. In this *capillarity-limited* regime, the kinetics follows with real units:

$$\tilde{l}^2 \simeq -2 \frac{\varphi_0}{\varphi_d - \varphi_0} \frac{\kappa \Psi_{\text{cap}}}{\eta_w} \tilde{t}, \quad (32)$$

and does not depend neither on the ambient relative humidity (RH) nor on the external mass transfer (J_0). For $\alpha > -\log(RH)$, the square root slowing down is due to the decrease of the evaporation driving force ($\Psi^* \simeq \Psi_{\text{ext}}$) leading to a *flow-limited* regime which follows with real units:

$$\tilde{l}^2 \simeq -2 \frac{\varphi_0}{\varphi_d - \varphi_0} \frac{\kappa \Psi_{\text{ext}}}{\eta_w} \tilde{t}. \quad (33)$$

In this regime, the growth rate does not depend again on external mass transfer conditions (J_0), but still depends on the imposed relative humidity through Ψ_{ext} .

3.3 A model case: monodisperse hard-sphere colloids

To illustrate the results of our model by numerical applications and to validate the assumptions made previously, we now use relations for monodisperse hard-sphere colloids of radius a . For such colloidal interactions, directional drying accumulates the colloids at the tip of the cell up to the random close-packing at volume fraction $\varphi_d \simeq 0.64$. We therefore implicitly assume, for simplicity, that colloids do not crystallize into an ordered network, either because of a slight polydispersity or because the crystallization kinetics is slower than the colloid accumulation rate.

For such randomly-packed assembly of hard-spheres, the mean pore radius r_p is defined as twice the ratio of pore volume to surface area:^{46,47}

$$r_p = \frac{2}{3} \frac{1 - \varphi_d}{\varphi_d} a, \quad (34)$$

$r_p \simeq 0.375a$ for $\varphi_d \simeq 0.64$. Different expressions exist for estimating the maximal capillary pressure Ψ_{cap} before recession of menisci, and we will assume as in Ref.⁴⁸ for the case of fully wetted particles:

$$\Psi_{\text{cap}} = -\frac{2\gamma}{r_p} = -\frac{3\varphi_d}{1 - \varphi_d} \frac{\gamma}{a}, \quad (35)$$

leading to $\Psi_{\text{cap}} \simeq -5.33\gamma/a$ for $\varphi_d \simeq 0.64$.

Finally, we chose to estimate the permeability of the randomly-packed assembly of colloids by the Carman-Koseny relation:⁴⁷

$$\kappa = a^2 \frac{(1 - \varphi_d)^3}{45\varphi_d^2}. \quad (36)$$

3.3.1 Validity of Eq. (17)

Peppin et al. described the dynamics of the solidification of hard-sphere colloidal suspensions in the experiment described in Fig. 1 taking into account the transport of the colloids by advection and diffusion.^{34,35} In these models, Eq. (17) can be demonstrated strictly from the colloid mass conservation but for a constant evaporation rate J . This is due to the existence of a steady solution of the advection-diffusion model governing the colloid con-

centration, in the reference frame of the growth of the packing. For a non-constant J , there is no such steady solution a priori, and Eq. (17) is only an approximation.

Nevertheless, Eq. (17) remains a good approximation as long as the temporal variation of the colloid concentration field for $x < -l$ can be neglected. For quasi-static conditions and negligible buoyancy,⁴⁹ the colloid concentration upstream the growing front can be approximated by the exponential decay $\varphi(x, t) \simeq \varphi_0 + (\varphi_d - \varphi_0) \exp[(x+l)/l_g]$, with $l_g = D/J$ and D the collective diffusion coefficient of the dispersion, well approximated by the Stokes-Einstein relation for hard-spheres.³⁴ The colloid mass balance, now taking into account the temporal variation of this colloid concentration profile leads to:

$$(\varphi_d - \varphi_0) \left(\frac{dl}{dt} + \frac{dl_g}{dt} \right) = \varphi_0 J. \quad (37)$$

The approximate colloid mass balance Eq. (17) comes from Eq. (37) when $\frac{dl_g}{dt} \ll \frac{dl}{dt}$, equivalently when:

$$D \ll -\frac{\kappa \Psi^*}{\eta_w}, \quad (38)$$

using $l_g = D/J$, Eqs. (11) and (16), with either $\Psi^* = \Psi_{\text{ext}}$ or $\Psi^* = \Psi_{\text{cap}}$ depending on the regime considered. Relations (35) and (36) then show that Eq. (38) is always fulfilled for hard-spheres over a wide range of radii a , and that Eq. (17) can be safely used to describe the growth rate. Moreover, these numerical applications show that the term $\frac{\kappa \Psi^*}{\eta_w}$ in Eq. (38) is very large. It is thus very likely that Eq. (17) remains valid even for colloids with long-range repulsive interactions, such as those often studied in the works cited previously,^{17,18,20,22,37} and for which colloidal interactions are known to enhance the collective diffusion coefficient D .^{27,50}

3.3.2 Validity of $\Gamma \gg 1$

The capillarity-limited growth described in particular by Eqs. (16) and (32) follows from $\Gamma \gg 1$ with Γ given by Eq. (15). The calculation of Γ requires nevertheless to estimate the effective diffusion coefficient of the water vapor in the porous packing D_w^p .

The regime of vapor diffusion within the pores of the colloidal packing depends on the value of the Knudsen number defined as $\text{Kn} = \lambda/r_p$, with λ the mean free path in air ($\lambda \simeq 64\text{--}68$ nm at room conditions⁵¹ in the range $\text{RH} = [0\text{--}1]$). Using Eq. (34), the transition $\text{Kn} = 1$ corresponds to radii $a \simeq 170\text{--}180$ nm. For $\text{Kn} \ll 1$, there are different theoretical estimates of the effective gas diffusion coefficient in a porous medium depending on its 3D morphology.⁵² We chose the following relation:

$$D_w^{p,n} \simeq \frac{2(1-\varphi_d)}{2+\varphi_d} D_w^{\text{air}}, \quad (39)$$

derived by Neale and Nader,⁵³ that gives good estimates for homogeneous and isotropic assemblies of spheres, D_w^{air} being the diffusion coefficient in air. In the Knudsen regime, $\text{Kn} \gg 1$, Huizenga and Smith⁴⁶ showed using measurements on randomly close-packings of monodisperse silica colloids, that the effective diffu-

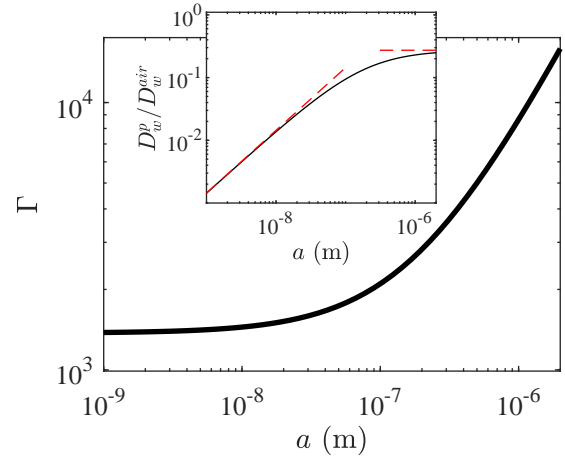


Fig. 6 Γ defined by Eq. (15) versus colloid radius a , estimated with the relations for hard-spheres given in Sec. 3.3. Inset: effective diffusion coefficient D_w^p of the vapor in the porous medium versus a , see Eq. (41). The dotted line at low a corresponds to Knudsen diffusion Eq. (40), and the one at large a to effective diffusion given by Eq. (39).

sion coefficient follows:

$$D_w^{p,k} \simeq \frac{1-\varphi_d}{\tau} \frac{4r_p}{3} \sqrt{\frac{2RT}{\pi M_w}}, \quad (40)$$

with the tortuosity $\tau \simeq 1.47 \pm 0.1$ and M_w the molar mass of water. To cover a wide range of colloid radius a , and thus of Knudsen number, we finally estimate the effective diffusion coefficient D_w^p by:

$$\frac{1}{D_w^p} = \frac{1}{D_w^{p,n}} + \frac{1}{D_w^{p,k}}, \quad (41)$$

as done for instance in Ref.⁵⁴, see the inset of Fig. 6.

Figure 6 shows Γ estimated using Eqs. (35), (36), and (41) versus the colloid radius a for $T = 22^\circ\text{C}$. These data show that $\Gamma \gg 1$ regardless of the size of the colloids. This numerical application validates the assumption done in Sec. 2.2.2 of minute recession of the menisci within the dense packing, and the existence of a capillarity-limited regime. Interestingly, Fig. 6 also shows that this assumption is a priori not due to Knudsen diffusion, at least for large colloids ($a > 100$ nm), a hypothesis often mentioned to explain the slowdown observed in confined drying experiments.^{18,36,37}

3.3.3 Numerical application of the model

We now illustrate the results of our model on a relevant experimental configuration: a microfluidic capillary of diameter $h = 25$ μm and centimetric length. For diffusion-limited transport from a flat air-water interface flush just with the outlet of the capillary, the mass transfer coefficient in Eq. (4) is:⁵⁵ $k \simeq 8D_w^{\text{air}}/(\pi h)$, leading to $J_0 \simeq 50$ $\mu\text{m/s}$ at $T = 22^\circ\text{C}$. Similar values of evaporation rates could be obtained with cells of larger cross-sectional dimensions, but with convection enhancing evaporation in the ambient air.

We use the relations given in Sec. 3.3 for hard-spheres to compute the crossover length l_c between the linear regime $l \propto t$ at

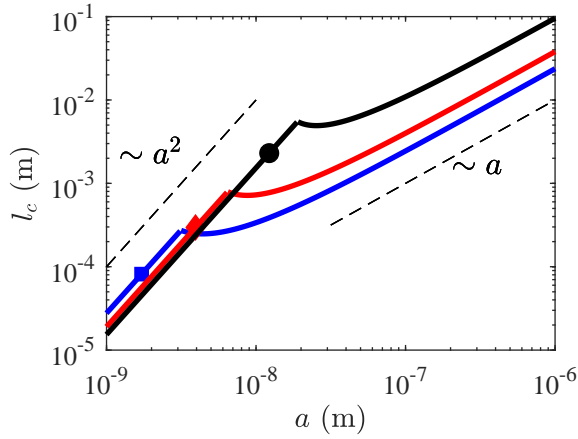


Fig. 7 Critical length l_c for the crossover between the linear growth $l \propto t$ and the square root growth $l \propto \sqrt{t}$ for the experimental conditions given in Sec. 3.3.3, and various relative humidity, RH = 0.2 (blue, ■), 0.5 (red, ◇), and 0.8 (dark, ●). The symbols show the critical radii below which the menisci do not recede, Eq. (24).

early times to the square root growth $l \propto \sqrt{t}$. In the flow-limited regime, $l_c = l_{\text{kel}}$ with l_{kel} given by Eq. (29), while $l_c = l_{\text{rec}}$ with l_{rec} given by Eq. (25) in the capillarity-limited regime. Figure 7 reports these data versus the colloid size a , for various RH (more precisely the minimal length between l_{kel} and l_{rec}). Figure 7 also shows for each RH, the critical radius a below which menisci are never expected to recede, see the criterion given by Eq. (24). This figure shows that most of the regimes predicted by the model are a priori expected to occur for colloids with radii ranging from $\simeq 5$ to $\simeq 100$ nm in a cell of centimetric length for the conditions of evaporation considered here. Interestingly, these data also reveal the important role played by RH on the transition between flow-limited and the capillarity-limited regimes, but also on the l_c values particularly in the latter regime.

Some experiments^{17,18,20,22,37} have measured l_c , in particular for silica colloids of small size $a \leq 20$ nm (Ludox dispersions). Unfortunately, the relative humidity was not a control parameter in these experiments, and was not often even reported. Dufresne *et al.* have also reported non-linear variations of l_c with a in the range $a = 6\text{--}26$ nm.¹⁷ The scaling laws shown in Fig.7, $l_c \sim a^2$ in the flow-limited regime and $l \sim a$ in the capillarity-limited regime, could maybe explain these results. As shown by our model, only the control of the relative humidity in these experiments would help to test this assumption.

4 Conclusions

In this work, we have developed a model to describe the dynamics of the consolidated front in confined directional drying experiments of colloidal dispersions. This model predicts at long times, a square root slowdown, $l \propto \sqrt{t}$, with two different origins: a flow-limited regime linked to the Kelvin effect and a capillarity-limited regime due to the recession of the evaporation interface. Our model also clarifies various assumptions commonly used in this context, and shows that Knudsen diffusion is not strictly at the origin of the capillarity-limited regime, as the latter can a priori

also be observed for large colloid sizes, see Fig. 6.

Beyond these results, our model highlights the importance of controlling the evaporation conditions in these experiments, and in particular the relative humidity RH. A control of the relative humidity would indeed allow to discriminate between the regime limited by capillarity, whose growth rate does not strictly depend on RH, and the regime limited by the flow showing a dependence with RH through Ψ_{ext} , see Eq. (33). Interestingly, the evaporation rate through the colloidal packing in the capillarity-limited regime is independent of RH, see Eq. (16). This was also demonstrated by Vincent *et al.* with experiments on drying-induced flows through a nano-porous silicon layer.⁴⁰ This humidity-insensitive water evaporation is reminiscent of recent results for molecular mixtures,^{56,57} but originates here in subtle couplings between evaporation, capillarity and vapor diffusion, as for example also in Ref.⁵⁸

Importantly, no experiment have reported, to our knowledge, even the minimal recession of the drying interface within the colloidal packing in the regime of square root growth $l \propto \sqrt{t}$, observed particularly with colloids of small radii, $a \leq 20$ nm.^{17,18,20,22,37} This result could suggest that the flow-limited regime is at the origin of these observations, but would deserve more precise local experimental measurements to confirm it. Furthermore, the capillarity-limited regime shares many similarities with the drying of a porous medium, for which the Kelvin effect can also play an important role.^{45,59} Local measurements of the water content in the colloidal packing (saturation) as done for instance in Ref.⁴⁵ using magnetic resonance imaging would also be a major asset for confined directional drying experiments.

Also, the high values of water potential Ψ^* due to the flow induced by evaporation are associated with tensile stresses that are often released in the experiments by the appearance of fractures,^{16–20} or the delamination of the packing from the cell walls.^{22,23} The model discussed in this article does not take these different phenomena into account at all, and it seems crucial to us to evaluate their role on the transport of water by evaporation and on the different regimes predicted by the model.

Finally, the confined directional drying configuration described in this work shares strong similarities with the important problem of colloid accumulation and clogging during drying of a porous medium^{60–63}, for which Fig. 1 could locally describe the pore-scale dynamics. Here again, the main ingredients of our model and some of its results could a priori also apply to these cases, and in part explain the global drying dynamics of colloidal dispersions in porous media.

Acknowledgements

We acknowledge Solvay, CNRS and the ANR program Grant No. ANR-18-CE06-0021 for financial support.

Notes and references

- 1 J. L. Keddie and A. F. Routh, *Fundamentals of latex film formation. Processes and Properties*, Springer, 2010.
- 2 J. Li, J. Fleetwood, W. B. Hawley and W. Kays, *Chem. Rev.*, 2022, **122**, 903–956.
- 3 W. B. Russel, *AIChE*, 2011, **57**, 1378–1385.

- 4 A. F. Routh, *Rep. Prog. Phys.*, 2013, **76**, 046603–046632.
- 5 L. Goehring, A. Nakahara, T. Dutta, S. Kitsunezaki and S. Tarafdar, *Desiccation Cracks and their Patterns: Formation and Modelling in Science and Nature*, Wiley-VCH, 2015.
- 6 P. Bacchin, D. Brutin, A. Davaille, E. Di Giuseppe, X. D. Chen, I. Gergianakis, F. Giorgiutti-Dauphiné, L. Goehring, Y. Hallez, R. Heyd, R. Jeantet, C. Le Floch-Fouéré, M. Meireles, E. Mittelstaedt, C. Nicloux, L. Pauchard and M.-L. Saboungi, *Eur. Phys. J. E*, 2018, **41**, 94–127.
- 7 A. F. Routh and W. B. Russel, *AIChE*, 1998, **44**, 2088–2098.
- 8 L. Goehring, W. J. Clegg and A. F. Routh, *Langmuir*, 2010, **26**, 9269–9275.
- 9 A. F. Routh and W. B. Zimmerman, *Chem. Eng. Sci.*, 2004, **59**, 2961–2968.
- 10 A. Lesaine, D. Bonamy, C. L. Rountree, G. Gauthier, M. Impéror-Clerc and V. Lazarus, *Soft Matter*, 2021, **17**, 1589–1600.
- 11 F. Boulogne, F. Giorgiutti-Dauphiné and L. Pauchard, *Soft Matter*, 2013, **9**, 750–757.
- 12 B. Sobac, Z. Larbi, P. Colinet and B. Haut, *Colloids Surf., A*, 2019, **576**, 110–122.
- 13 E. Lintingre, F. Lequeux, L. Talini and N. Tsapis, *Soft Matter*, 2016, **12**, 7435–7444.
- 14 A. Bouchaudy and J.-B. Salmon, *Soft Matter*, 2019, **15**, 2768–2781.
- 15 H. Gelderblom, C. Diddens and A. Marin, *Soft Matter*, 2022, **18**, 8535–8553.
- 16 C. Allain and L. Limat, *Phys. Rev. Lett.*, 1995, **74**, 2981–2984.
- 17 E. R. Dufresne, E. I. Corwin, N. A. Greenblatt, J. Ashmore, D. Y. Wang, A. D. Dinsmore, J. X. Cheng, X. Xie, J. W. Hutchinson and D. A. Weitz, *Phys. Rev. Lett.*, 2003, **91**, 224501–224504.
- 18 E. R. Dufresne, D. J. Stark, N. A. Greenblatt, J. X. Cheng, J. W. Hutchinson, L. Mahadevan and D. A. Weitz, *Langmuir*, 2006, **22**, 7144–7147.
- 19 G. Gauthier, V. Lazarus and L. Pauchard, *Langmuir*, 2007, **23**, 4715–4718.
- 20 S. Inasawa and Y. Yamaguchi, *Soft Matter*, 2012, **8**, 2416–2422.
- 21 Z. Niu, H. Gao, M. Doi, J. Zhou and Y. Xu, *Langmuir*, 2022, **38**, 13880–13887.
- 22 A. Sarkar and M. S. Tirumkudulu, *Soft Matter*, 2011, **7**, 8816–8822.
- 23 Y. Xu, G. K. German, A. F. Mertz and E. R. Dufresne, *Soft Matter*, 2013, **9**, 3735–3740.
- 24 P. Kiatkirakajorn and L. Goehring, *Phys. Rev. Lett.*, 2015, **115**, 088302–088306.
- 25 B. Yang, N. D. Smith, A. Johannes, M. Burghammer and M. Smith, *Sci. Rep.*, 2018, **8**, 12979–12987.
- 26 A. Sarkar and M. S. Tirumkudulu, *Langmuir*, 2009, **25**, 4945–4953.
- 27 L. Goehring, J. Li and P.-C. Kiatkirakajorn, *Phil. Trans. R. Soc. A*, 2017, **375**, 20160161–20160183.
- 28 K. Inoue and S. Inasawa, *RSC Advances*, 2020, **10**, 15763–15768.
- 29 E. Hooiveld, H. M. van der Kooij, M. Kisters, T. E. Kodger, J. Sprakel and J. van der Gucht, *J. Colloid Interface Sci.*, 2023, **630**, 666–675.
- 30 F. Boulogne, L. Pauchard, F. Giorgiutti-Dauphiné, R. Botet, R. Schweins, M. Sztucki, J. Li, B. Cabane and L. Goehring, *Europhys. Lett.*, 2014, **105**, 38005–38010.
- 31 C. Noirjean, M. Marcellini, S. Deville, T. E. Kodger and C. Monteux, *Phys. Rev. Materials*, 2017, **1**, 065601–065610.
- 32 J. You, J. Wang, L. Wang, Z. Wang, Z. Wang, J. Li and X. Lin, *Colloids Surf., A*, 2017, **531**, 93–98.
- 33 S. Inasawa, Y. Oshimi and H. Kamiya, *Soft Matter*, 2016, **12**, 6851–6857.
- 34 S. S. Peppin, J. A. Elliott and M. G. Worster, *J. Fluid Mech.*, 2006, **554**, 147–166.
- 35 R. W. Style and S. S. Peppin, *Proc. R. Soc. London, Ser. A*, 2011, **467**, 174–193.
- 36 K. J. Wallenstein and W. B. Russel, *J. Phys.: Condens. Matter*, 2011, **23**, 194104–194109.
- 37 P. Lidon and J.-B. Salmon, *Soft Matter*, 2014, **10**, 4151–4161.
- 38 R. Tatsumi, O. Koike, Y. Yamaguchi and Y. Tsuji, <https://doi.org/10.48550/arXiv.2201.12992>.
- 39 W. B. Russel, D. A. Saville and W. R. Schowalter, *Colloidal dispersions*, Cambridge University Press, 1989.
- 40 O. Vincent, A. Szenicer and A. D. Stroock, *Soft Matter*, 2016, **12**, 6656–6661.
- 41 B. R. Bird, E. W. Stewart and E. N. Lightfoot, *Transport phenomena*, John Wiley & Sons, New York, 2002.
- 42 *Wolfram MathWorld*, <https://mathworld.wolfram.com/LambertW-Function.html>.
- 43 P. Lehmann, S. Assouline and D. Or, *Phys. Rev. E*, 2008, **77**, 056309–056324.
- 44 J. B. Laurindo and M. Prat, *Chem. Eng. Sci.*, 1996, **51**, 5171–5185.
- 45 J. Thiery, S. Rodts, D. A. Weitz and P. Coussot, *Phys. Rev. Fluids*, 2017, **2**, 074201–074215.
- 46 D. G. Huizenga and D. M. Smith, *AIChE*, 1986, **32**, 1–6.
- 47 B. J. Rogers and M. J. Wirth, *ACS Nano*, 2013, **7**, 725–731.
- 48 L. R. White, *J. Colloid Interface Sci.*, 1982, **90**, 536–538.
- 49 J.-B. Salmon and F. Doumenc, *Phys. Rev. Fluids*, 2020, **5**, 024201–024219.
- 50 B. Sobac, S. Dehaeck, A. Bouchaudy and J.-B. Salmon, *Soft Matter*, 2020, **16**, 8213–8225.
- 51 S. Jennings, *J. Aerosol Sci.*, 1988, **19**, 159–166.
- 52 D. Mu, Z. S. Liu, C. Huang and N. Djilali, *J. Porous Mater.*, 2007, **14**, 49–54.
- 53 G. H. Neale and W. K. Nader, *AIChE*, 1973, **19**, 112–119.
- 54 D. Mu, Z. S. Liu, C. Huang and N. Djilali, *Microfluid. Nanofluid.*, 2008, **4**, 257–260.
- 55 B. Dollet and F. Boulogne, *Phys. Rev. Fluids*, 2017, **2**, 053501–053510.
- 56 J.-B. Salmon, F. Doumenc and B. Guerrier, *Phys. Rev. E*, 2017, **96**, 032612–032625.

- 57 K. Roger, E. Sparr and H. Wennerström, *Phys. Chem. Chem. Phys.*, 2018, **20**, 10430–10438.
- 58 J. C. Eijkel, B. Dan, H. W. Reemeijer, D. C. Hermes, J. G. Bomer and A. Van Den Berg, *Phys. Rev. Lett.*, 2005, **95**, 256107–256110.
- 59 O. Maalal, M. Prat and D. Lasseux, *Phys. Fluids*, 2021, **33**, 027103–027117.
- 60 E. Keita, P. Faure, S. Rodts and P. Coussot, *Phys. Rev. E*, 2013, **87**, 62303–62308.
- 61 J. Zürcher, B. R. Burg, L. Del Carro, A. R. Studart and T. Brunschwiler, *Transp. Porous Media*, 2018, **125**, 173–192.
- 62 F. Qin, A. Mazloomi Moqaddam, Q. Kang, D. Derome and J. Carmeliet, *Transp. Porous Media*, 2019, **128**, 929–943.
- 63 E. Ghiringhelli, M. Marcoux, S. Geoffroy and M. Prat, *Colloids Surf., A*, 2023, **656**, 130432–130441.